ELSEVIER

Organic Electronics 2 (2001) 121–134

Organic Electronics

www.elsevier.com/locate/orgel

Combined LEED and STM study of PTCDA growth on reconstructed Au(1 1 1) and Au(1 0 0) single crystals

S. Mannsfeld *, M. Toerker, T. Schmitz-Hübsch, F. Sellam, T. Fritz, K. Leo

Institut für Angewandte Photophysik, Technische Universität Dresden, 01062 Dresden, Germany

Received 12 February 2001; received in revised form 3 July 2001; accepted 3 July 2001

Abstract

The growth of perylene-3,4,9,10-tetracarboxylic-3,4,9,10-dianhydride (PTCDA) thin films on the reconstructed surfaces of Au(1 1 1) and Au(1 0 0) single crystals was investigated with low energy electron diffraction and scanning tunneling microscopy under ultrahigh vacuum conditions. The samples were prepared by means of the organic molecular beam epitaxy (OMBE) technique. Two phases with molecular arrangements resembling the (1 0 2) plane herringbone structure of the PTCDA bulk crystal are found on Au(1 1 1); one of them is observed at higher deposition rates only. Both herringbone phases grow homogeneously in large domains on top of the alternating domains of the well known $(22 \times \sqrt{3})$ Au(1 1 1) surface reconstruction. We show that this surprising growth behavior can be explained using the point-on-line coincidence concept. On the reconstructed Au(1 0 0) surface, we observe various orientations of a herringbone phase. Again the different orientations of this phase are point-on-line coincident, this time with the almost hexagonal $\mathrm{Au(1\,0\,0)_{hex}}$ surface reconstruction. Besides the herringbone phases we regularly observe a square phase of PTCDA on both substrate surfaces.

Keywords: Organic thin films; PTCDA; Low energy electron diffraction; Scanning tunneling microscopy; Molecular beam epitaxy

1. Introduction

Organic molecular dyes show high and spectral selective absorption, but often also have semiconductor properties. To achieve good transport properties in devices composed of organic molecules, highly ordered thin films are important. The high order of a crystalline film increases the effective charge carrier mobility. Furthermore, a defined crystalline structure makes it also easier to understand the optical and electronic properties of these organic materials.

To achieve the growth of molecules in large, highly ordered domains, it is necessary to gain detailed insight into the mechanisms of molecular ordering and the possibilities to control the growth by appropriate choice of parameters like substrate symmetry or deposition rate, etc. Still too little is known about the complicated growth kinetics. Hence, the investigations of organic molecular epitaxy are still in a descriptive stage. One appropriate technique to create highly ordered organic molecular films is molecular beam epitaxy (MBE) [1]. This technique allows an investigation of the film properties under ultrahigh vacuum (UHV)

* Corresponding author. Tel.: +49-351-4633504; fax: +49-351-4637065.

E-mail address: mannsfel@iapp.de (S. Mannsfeld).

1566-1199/01/$ - see front matter
PII: S1566-1199(01)00018-0

conditions with analysis methods such as scanning tunneling microscopy (STM) or low energy electron diffraction (LEED).

Many of the studies published deal with the deposition of a single molecular species on an inorganic substrate of metallic, semiconducting or dielectric nature. Perylene-3,4,9,10-tetracarboxylic-3,4,9,10-dianhydride (PTCDA) has been widely used as a model substance to study the epitaxial growth of organic films on metallic or semiconducting substrates. In most cases, the PTCDA molecules forming the molecular layer exhibit the herringbone arrangement which is characteristic for the (1 0 2) plane of the bulk crystal, e.g., on HOPG [2–6], Au(1 0 0) [8–10], Ag(1 1 0) [11], Cu(1 0 0) [12], MoS_2 [4,12,13], Si [14], NaCl [15], or even heterogeneously grown on top of the organic molecule hexa-peri-hexabenzocoronene (HBC) [16]. However, adsorbate lattice configurations which differ from the arrangement of molecules in the (1 0 2) plane were found as well, e.g. on the Ag(7 7 5) [17], Ag(1 1 0) [18,19], Cu(1 0 0) [12], Au(1 0 0) surfaces [7], or embedded in a thiol layer [20].

If the influence of a crystalline substrate on the growth of an ordered molecular layer shall be investigated, the primary question is whether there is any match between the two lattices or not. For the large planar aromates like PTCDA, the so-called point-on-line coincidence turned out to be a typical growth mode [2,3,21], especially on substrates which do not interact site-specific with the adsorbate molecules, i.e, in cases when the intermolecular interactions are determinant for the arrangement of molecules within the adsorbate layer.

While the lattice constants for PTCDA on reconstructed Au(1 1 1) were known before [8], the relations between the molecular lattices and underlying substrate lattice have not been sufficiently discussed yet. In this contribution we do not only explain the homogeneous growth of PTCDA in single domains on top of different Au(1 1 1) surface reconstruction domains with point-on-line epitaxy, we also demonstrate the applicability of the point-on-line coincidence concept for PTCDA on reconstructed Au(1 0 0), i.e., on a chemically identical but crystallographically different substrate surface. PTCDA on Au(1 0 0) was previously investigated on vapor deposited gold layers on KBr, but was mainly found to grow in a rod-like phase, and the well-known herringbone phase was only found on unreconstructed parts of the Au(1 0 0) surface [7].

2. Experimental

All experiments were carried out under UHV conditions in a three-chamber OMBE device described elsewhere [16]. Au(1 1 1) and Au(1 0 0) single crystals (cutting angle accuracy $\pm 0.1°$) were used as substrates. Before the deposition of PTCDA, the substrates were prepared by repeated cycles of argon ion bombardment (600 eV, 30 min) and subsequent annealing (870 K, 30 min). The surface was checked for the reconstruction with STM and LEED. PTCDA (Aldrich) was purified twice by gradient sublimation and evaporated from a Knudsen-like effusion cell after thorough degassing (>1 h at 520 K). The higher of the two deposition rates used (2.5 ML/min) was calibrated by optical investigation while the lower deposition rate of $\sim$0.5 ML/min was determined by the comparison of both rates using a quartz microbalance. PTCDA was deposited onto the Au crystals at room temperature with the pressure in the chamber being about 3×10^{-9} mbar during the deposition.

Samples of submonolayer coverage of PTCDA as well as samples with more than monolayer coverage were produced and investigated with STM and LEED. LEED (Omicron SPECTA-LEED) images were taken at low emission current (to minimize potential damage of the adsorbate layer) and recorded with a CCD camera. To enable accurate measurements, the curvilinear image distortion introduced by the camera lens system was corrected by recording LEED images of the well known (7×7) surface reconstruction of Si(1 1 1). Despite this correction, the lattice constants determined by LEED measurements were found to be systematically too small in the low voltage region. By calibration for low electron beam voltages as suggested by Günther [22] we found a constant voltage display error of

$\Delta U = -1.3 \pm 0.1$ V, which is close to the value he obtained. A possible reason for this error could be a difference in the work functions of the electron emitting filament and the grids of the LEED optics [22].

STM images were obtained with an UHV scanning tunneling microscope (Omicron STM/AFM). The tunneling tips used in these experiments were etched electrochemically in NaOH solution from tungsten wire and rinsed in distilled water and ethanol. Before transfer to the STM chamber, oxygen and other contaminants were removed from the tip surface in UHV by argon ion bombardment and subsequent annealing up to 870 K for 30 min. STM images are usually subject to distortion caused by thermal drift and piezo-creep. Therefore, they have not been used for precise determination of lattice parameters, but for investigation of the molecular arrangement only. However, the STM images shown herein have been scaled using lattice dimension data from LEED. To scale a STM image this way, an adsorbate structure in the STM image has to be identified with a structure measured in corresponding LEED images. This was possible for all STM images because the discrepancy between lengths and angles in STM images and the respective values from LEED measurements was small enough to allow an unequivocal identification. By comparing the dimensions of an identified structure from STM and LEED measurements, a scaling matrix can be calculated. This matrix is then applied to the STM image using standard image processing software.

After investigation of the as-deposited layers, the samples were annealed up to 510 K for 10–20 min to study the possible influence of this treatment on the adsorbate layer structures.

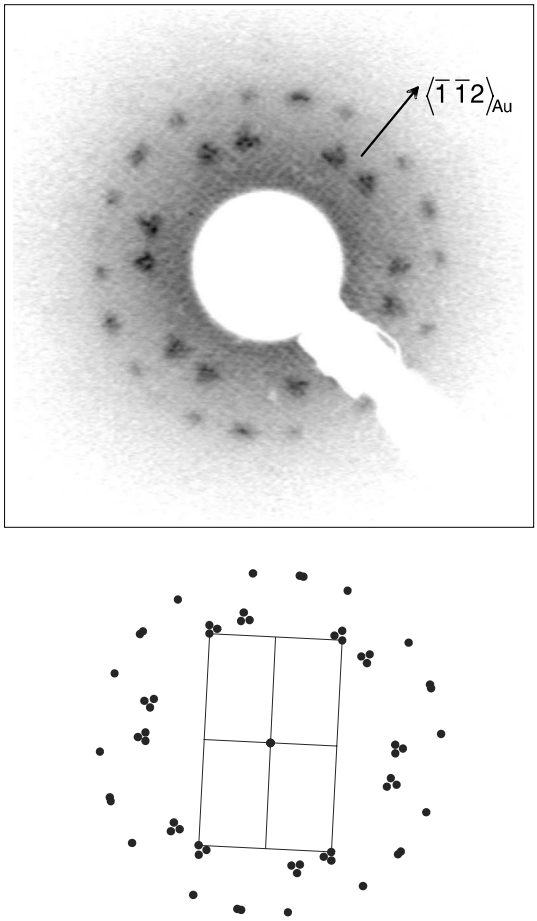

Fig. 1. LEED image of a submonolayer coverage (~0.5 ML) of PTCDA on Au(1 1 1) (prepared at a deposition rate of about 0.5 ML/min), obtained at a electron energy of $E_0 = 20.6$ eV. The diffraction pattern can be explained by six symmetry equivalent domains of a herringbone phase. The (0 1) and (1 0) spots are missing due to p2gg symmetry of the adsorbate lattice. In the lower part, a geometrically calculated diffraction pattern for the assumed structural model can be seen.

3. Results and discussion

3.1. PTCDA on reconstructed Au(1 1 1)

Here, we discuss the results for PTCDA layers on a Au(1 1 1) single crystal. LEED images taken from samples with about half a ML coverage of PTCDA prepared at a deposition rate of 0.5 ML/min (Fig. 1) can be explained by a superposition of six symmetry-equivalent domains of a rectangular adsorbate structure, referred to as Phase H1 in the following. The number of six domains can be easily understood by considering the growth of PTCDA on top of the reconstruction. There are three equivalent domains of the $(22 \times \sqrt{3})$ surface reconstruction; for adsorbate structures which are not aligned with the reconstruction lattice axes there are two additional

symmetry equivalent mirror domains. Although we have not obtained images in which these spots appeared clearly resolved, it was essential for an explanation of the LEED pattern in Fig. 1 to assume the triangular shaped diffraction features to consist of three spots.

In addition to the spots of Phase H1, new spots appeared in LEED images for samples prepared with an increased deposition rate of about 2.5 ML/min (Fig. 2). These spots can be explained with six symmetry-equivalent domains of another rectangular adsorbate lattice, denoted as Phase H2 in the following. Although we sometimes observe very weak diffraction spots of Phase H2 also for samples prepared with a deposition rate of 0.5 ML/min, they do not appear as intense as those of Phase H1, i.e., the surface fraction covered by Phase H2 is much smaller compared to that of Phase H1, unless the sample was prepared with the higher molecular flux. This is in agreement with the results of annealing experiments performed subsequently. After annealing of the sample at 470 K for 10 min, only Phase H1 was visible in the LEED image again. The higher molecular flux limits diffusion and migration processes which obviously leads to the formation of a phase which is energetically slightly less advantageous than Phase H1.

The triangles in the diffraction pattern of Phase H2 differ in size from the corresponding triangles of Phase H1, indicating a difference in the lattice constants. With the angle $\delta = \angle(\vec{a},\ [\bar{1}\,\bar{1}\,2]_{\mathrm{Au}})$ describing the azimuthal relation between the adsorbate lattice and the substrate lattice, the following lattice parameters were obtained from LEED measurements: $\delta = 22.0° \pm 0.6°$, $a = 12.3 \pm 0.2$ Å, $b = 19.6 \pm 0.3$ Å, $\Gamma = 89.7° \pm 0.7°$ for Phase H1, and $\delta = 7.1° \pm 0.5°$, $a = 12.6 \pm 0.2$ Å, $b = 18.9 \pm 0.3$ Å, $\Gamma = 89.9° \pm 0.5°$ for Phase H2. The angle Γ denotes the angle between the in-plane adsorbate lattice vectors. Although these lattice constants are similar, H1 and H2 are treated as different phases since the difference in the lattice constant b is larger then the experimental error would allow to interpret H1 and H2 as two orientations of a single phase.

It is noteworthy that the angle δ can only be equivocally determined as either δ, $|\delta - 60°|$ or $|\delta + 60°|(|\delta - 120°|)$ because of the substrate symmetry. This means that adsorbate lattices with these different angles would all produce identical diffraction patterns which is another reason why STM investigation of the sample is required. There are systematic absences of spots in the observed diffraction patterns. The $(h\,0)$ spots as well as the $(0\,k)$ spots are missing for odd values of h and k

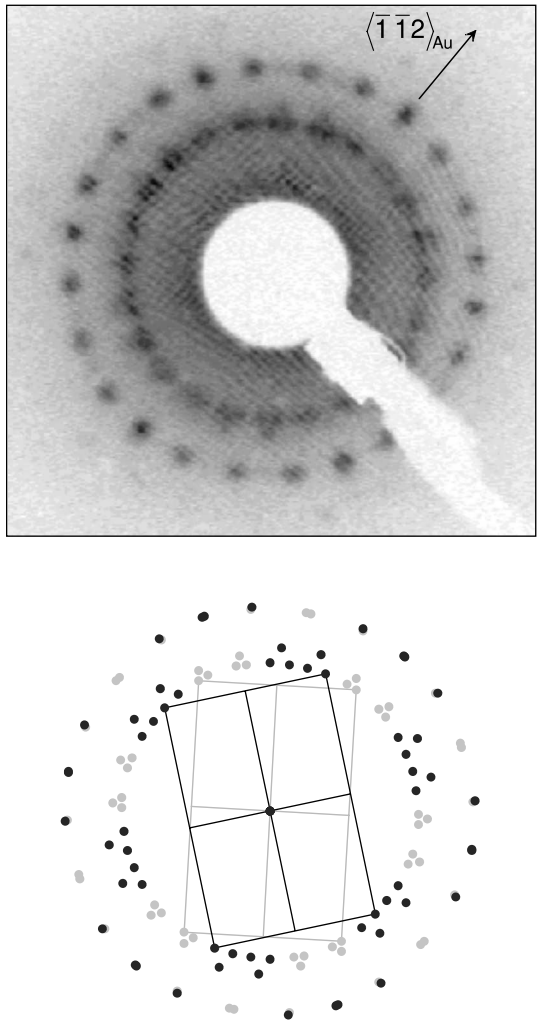

Fig. 2. LEED image of a sample of ~1 ML PTCDA on Au(1 1 1) prepared at a molecular flux of about 2.5 ML/min, taken at an electron energy of $E_0 = 14.7$ eV. The new spots in the diffraction pattern (black; the grey spots in the geometrically calculated LEED image correspond to Phase H1) can be explained by six symmetry equivalent domains of another herringbone Phase H2.

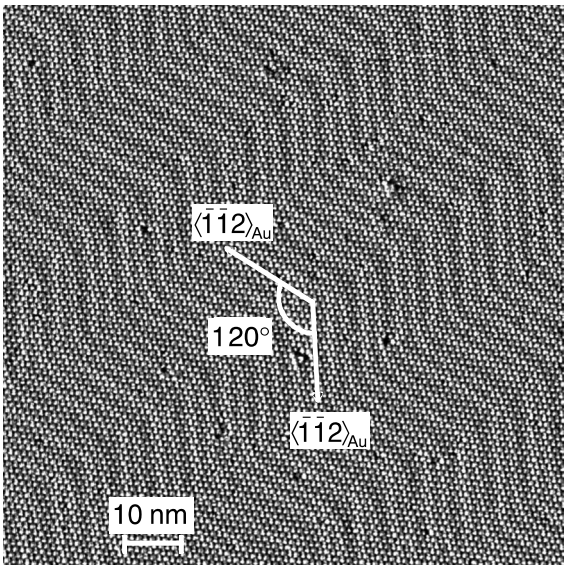

Fig. 3. Highly ordered and almost defect-free PTCDA domain of Phase H1, grown on a large and regularly reconstructed Au(1 1 1) terrace. The alternating bridging bends of the reconstruction are visible as a modulation in the molecular contrast of the PTCDA layer [$U = 0.71$ V, $I = 0.14$ nA].

which indicates the p2gg two-dimensional (2D) space-group symmetry for both adsorbate phases. This symmetry is confirmed by STM images (Fig. 3).

Both phases form extended, highly ordered, and almost defect-free domains of the well known PTCDA herringbone structure with two molecules per unit cell and a molecular arrangement which resembles that of the (1 0 2) plane in the bulk crystal. However, none of the two phases can be precisely classified as (1 0 2) bulk plane structure of the α- or β-PTCDA modification [23]. Instead, they are considered to be slightly distorted (1 0 2)-like phases. The strain within the molecular layer, calculated according to Fenter et al. [9] with the (1 0 2) plane of α- and β-PTCDA as references, is below 3% for both phases.

A zig-zag pattern, similar to that of the $(22 \times \sqrt{3})$ Au(1 1 1) surface reconstruction in which the bridging rows perform alternating 120° bends, can be seen as a modulation of the molecular contrast in the STM image. This provides evidence that the Au(1 1 1) surface reconstruction is not lifted upon deposition of PTCDA. Furthermore, STM images showing both covered and bare sample surface areas confirm that the reconstruction lattice is not changed by the adsorbed PTCDA layer. Therefore, the observed adsorbate domains have to be treated as growing on top of the $(22 \times \sqrt{3})$ reconstructed Au(1 1 1) lattice.

The homogeneous growth of PTCDA domains despite the changes in the substrate lattice underneath (represented by alternating reconstruction domains) questions, at the first glance, any influence of the reconstruction on the growth of PTCDA. We find that domains of the herringbone Phases H1 and H2 grow on top of the two possible configurations of the reconstruction bends (Fig. 4). The uniform growth of Phases H1 and H2 (like sketched in Fig. 4) requires a description with three azimuthal orientations, i.e, three angles $\delta_{1,2,3} = \angle(\vec{a},\ [\bar{1}\,\bar{1}\,2]_{\mathrm{Au}})$. For Phase H1 these are: $\delta_{1,2,3} = 22.0°,\ 38.0°,\ 82.0° \pm 0.6°$; for Phase H2 we find $\delta_{1,2,3} = 7.1°,\ 52.9°,\ 67.1° \pm 0.6°$. These orientations are, of course, identical to the equivocally determined angles resulting from LEED image measurements, because in both cases they are caused by the sixfold symmetry of the Au(1 1 1) plane.

An almost square phase (in the following called square phase for simplicity) with two molecules

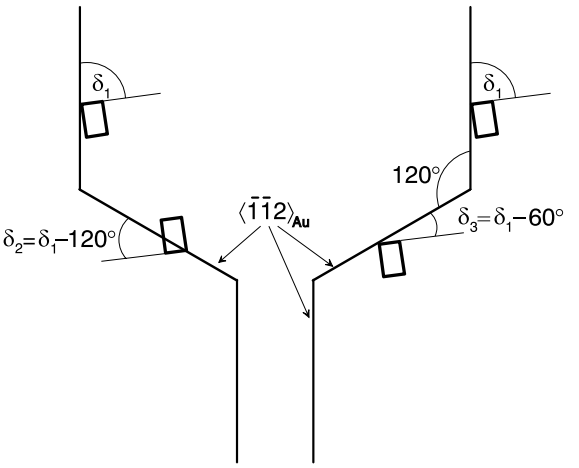

Fig. 4. Scheme for the single domain growth of the PTCDA herringbone phases (▭) on top of both possible configurations of Au(1 1 1) reconstruction zig-zag domains. A description of the azimuthal relation between adsorbate and substrate requires three angles for each phase $\delta_{1,2,3} = \angle(\vec{a}, [\bar{1}\,\bar{1}\,2]_{\mathrm{Au}})$.

per unit cell occurs in very small domains only and does, therefore, not appear in LEED images. Regardless of the deposition rate, we find two different orientations of the square phase S, S-1 and S-2, with the following lattice parameters: $\delta_{1,2} = 34°, 63° \pm 2°$, $a = 16.1 \pm 0.8$ Å, $b = 16.5 \pm 0.8$ Å, $\Gamma = 91° \pm 2°$. These lattice parameters were obtained from scaled STM images. Fig. 5 shows a small "patch" of S-1 embedded in a domain of the herringbone Phase H2. One of the square phase orientations (S-1) has been reported previously [10].

In contrast to the herringbone phases, our STM images do not clearly reveal the molecular arrangement in the square phase. However, sterical modeling with these lattice dimensions considering the van-der-Waals radii of the PTCDA molecules suggests a perpendicular in-plane arrangement of the two molecules in the unit cell. This is backed by the appearance of a similar structure on Au(1 0 0) (see below) and reasonable if the energy stored in the molecular layer is considered: a significantly different molecular arrangement would cause a considerable macroscopic quadrupole moment within the layer (because of the anhydride groups) which is energetically not favorable [22]. Unlike the Phases H1 and H2, the square phase S is not capable of growing on top of the alternating reconstruction domains, i.e., there is only one angle δ for each orientation. We always find the square domains to end abruptly at the kinks of the reconstruction Fig. 5.

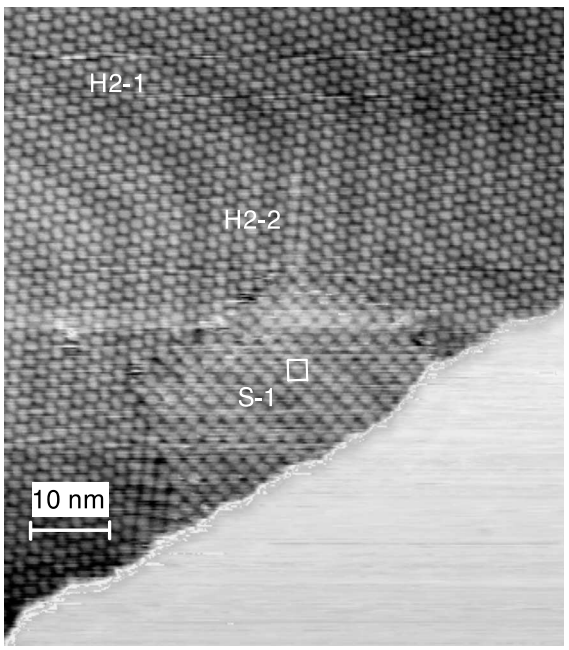

Fig. 5. A small domain of the S-1 orientation of the PTCDA square phase embedded in a domain of the herringbone Phase H2 on Au(1 1 1). Unlike the latter, we never find the square phase domains extending over more than one reconstruction domain of the substrate which indicates a definite influence of the surface reconstruction on the observed growth. A different color table was used for the lower right part (a bare gold terrace) to enhance image contrast [$U = 1.0$ V, $I = 0.18$ nA].

In the following, we want to discuss the mutual orientation between the adsorbate lattice and the substrate lattice. Orientations of the herringbone phase with angles δ of 22°, 55° and 39° were previously observed during STM investigations [8]. However, these results were obtained for vapor deposited gold films on mica instead of gold single crystals and did not provide evidence for the homogenous growth on top of the reconstruction domain sequences.

To decide whether the observed growth represents a certain type of epitaxy, it is useful to analyze the matrix relations between adsorbate lattice and substrate lattice. We use a special software EPITAXY [24] which is based on a geometrical lattice match model. This model was derived from an algorithm used by Hillier and Ward [25] which allows a qualitative discussion of the total potential energy of certain adsorbate systems based on the following assumptions: (i) the total potential energy of the system can be expressed as a sum of the respective lattice energies of adsorbate layer and substrate layer, and the energy resulting from the interaction between the molecules in the adsorbate layer and atoms in the substrate layer, (ii) the substrate is rigid, i.e., the lattice energy of the substrate is constant, (iii) the arrangement of the adsorbate molecules on the substrate lattice differs only slightly from a preferred molecular arrangement (small strain) which means that the lattice energy of the molecular layer is constant as well.

If these conditions are met, the variation of the total potential energy corresponds to the variation of the energy resulting from the interaction be-

tween the layers. This interaction energy was originally modeled by 2D cosine pseudopotentials [25], a method which has the huge advantage to lead to analytical terms and at least qualitative expressions for the total potential energy. However, for the important case of large (infinite) domain diameters we could show that this algorithm can be replaced by a simple analysis of the matrix relation between the adsorbate lattice and the substrate lattice [24,26]. In the software mentioned above, a hypothetical adsorbate lattice is rotated step-by-step with respect to the substrate lattice. At each step, the adsorbate surface mesh parameters are varied within predefined intervals. The matrix relation between the two lattices is analyzed for all resulting configurations. If a sufficient number of matrix elements are integers (within a predefined error span), the analyzed configuration is assumed to represent an epitaxial relation between adsorbate lattice and substrate lattice. The epitaxial relations are classified according to the definitions given by Hooks et al. [21]. Every epitaxial configuration found is regarded as a "hit" (or count) resulting in a histogram if the number of hits is plotted versus the angle between the two lattices.

One important result of the qualitative calculation of the potential energy with the cosine pseudopotentials is that there is an energetic gain not only in those cases in which the two lattices are in registry in two lattice directions. In the case of the so-called point-on-line coincidence, the adsorbate lattice points are situated on primitive lattice lines of the substrate rather than on substrate lattice points. This does not require an adsorbate basis vector to be parallel to a substrate lattice line but means that, starting from a substrate lattice point, both adsorbate basis vectors end on lattice lines parallel to the same primitive lattice line. In the reciprocal space this corresponds to the fact that one reciprocal substrate basis vector is a multiple of a reciprocal adsorbate basis vector. In the matrix relation, point-on-line coincidence is indicated by the fact that one column of the matrix consists of integers [21]. However, in the case of hexagonal (or almost hexagonal) lattices there are three primitive lattice lines which requires an appropriate choice of the substrate lattice basis in order to obtain such a column of integers in the matrix relation.

To account for the Au(1 1 1) surface reconstruction in the calculation, the lattice of the reconstructed surface was modeled as an Au(1 1 1) lattice, uniaxially compressed in the $[\bar{1}\,1\,0]_{\mathrm{Au}}$ direction [27]. It can then be simplified to $|\vec{s}_1| = |\vec{s}_2| = 2.8532$ Å and $\angle(\vec{s}_1, \vec{s}_2) = 57.8192°$. The histogram plot calculated with the software described above for the herringbone phases shows the number of matching point-on-line coincident configurations versus the angle δ (Fig. 6). No commensurate or point-on-point epitaxial relations were found within the scanned parameter range. The angles δ_{sim} at the peaks in the histogram are found to be in good agreement with the experimentally observed angles δ, enabling an assignment of the peaks to the observed orientations.

It has to be pointed out that a larger peak in such a histogram does not necessarily mean a higher probability to occur for the respective orientation. Instead, the differences in peak heights are mainly caused by the chosen step width of δ_{sim} and rounding errors. The peaks are labeled according to the phase and the index of the angle δ. During our investigations, we did not find orientations which could be associated with the remaining peaks in the histogram Fig. 6. Interestingly, Chizhov et al. report a herringbone phase orientation with an angle $\delta \sim 16°$ which is in good correspondence with one of the unassigned peaks in Fig. 6 [10].

For the herringbone phases in particular, one has to bear in mind that the three orientations $\delta_{1,2,3}$ of the phases H1 and H2 are equivalent by the rotational symmetry of the Au(1 1 1) plane, as they are caused by the homogeneous growth of large adsorbate domains on the symmetry equivalent reconstruction domains. We, therefore, looked for histogram hits with similar lattice dimensions in each of the three related peaks of a phase, rather than simply selecting hits whose angles δ_{sim} are in best agreement with the experimentally observed angles δ. The results listed in Table 1 represent the best compromise between calculated and experimental lattice dimensions and angles for all observed adsorbate lattices on reconstructed Au(1 1 1).

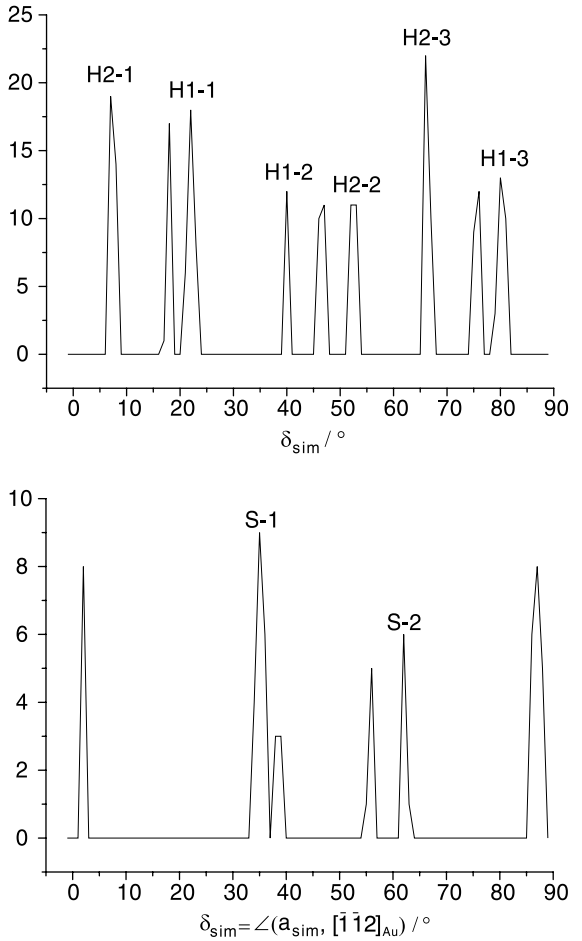

Fig. 6. Histogram showing the point-on-line coincident relations for the herringbone phases (upper chart) and the square phase (lower chart) with the model of the reconstructed Au(1 1 1) lattice. The scanned adsorbate lattice parameter range for the herringbone phases was: $a_{sim} = 12.0$–12.8 Å, $b_{sim} = 18.8$–19.8 Å, $\Gamma_{sim} = 89.5°$–$90.5°$. In case of the square phase, the lattice constants were varied between: $a_{sim} = 15.9$–16.3 Å, $b_{sim} = 16.3$–16.8 Å, $\Gamma_{sim} = 89°$ and $91°$. The peaks are labeled according to the respective phase and the index of the angle δ. The peak at an $\delta_{sim} \sim 16°$ might be related to an herringbone phase reported by Chizov et al. [10].

However, there are certain differences between experimental values and simulation values, e.g., the angle δ of orientation H1-2 obtained from the simulation differs from the measured angle by more than the corresponding experimental error. Moreover, we have to state that for both herringbone phases, H1 and H2, it is impossible to find a entirely point-on-line coincident set of orientations δ_{sim}, $\delta_{sim} - 60°$, $\delta_{sim} + 60°$ within the error intervals of the respective measured lattice parameters a, b, γ of H1 and H2. Therefore, the question arises whether the point-on-line concept is an adequate description for the observed growth at all. There are two possibilities to answer that question:

(i) If we assume that the growth of the PTCDA is in fact governed by point-on-line coincidence, the large herringbone phase domains cannot be homogeneous, i.e., the surface mesh has to vary slightly in areas of different reconstruction domains. We can, however, exclude such a variation of the surface mesh because the FFT spectra of our STM images show a high number of orders with sharp spots. Alternatively, the differences between experimental values and simulation might be caused by the model for the reconstructed surface lattice which is simplified compared to the complicated lattice structure of the surface reconstruction. The description as uniaxially densified Au(1 1 1) surface layer disregards the vertical displacement of gold atoms and the slightly sinusoidal lattice line within the actual rectangular $(22 \times \sqrt{3})$ unit cell of the surface reconstruction [28].

(ii) On the other hand one has to consider that the matrix relations listed in Table 1 represent point-on-line coincident solutions which are exact in a mathematical sense while real substrate lattice lines will certainly have a finite width. Therefore, in reality there could either be a general slight deviation from the exact point-on-line coincident growth, or a larger difference in one part of the PTCDA herringbone phase domains could be compensated by a ''better'' match in another part (different parts of the PTCDA domains refer to the different reconstruction domains in the substrate layer). In these cases the growth could still be described as point-on-line coincident, considering that point-on-line coincidence is a lattice match model based on mathematically exact lattices and does, therefore, not reflect all the energetic influences involved in the actual ordering process.

Taking these restrictions into account, we conclude that the growth of herringbone domains on top of the reconstruction is homogeneous because

Table 1
Lattice parameters of the PTCDA phases and orientations found on reconstructed Au(1 1 1), compared to the respective results obtained from the simulation

Phase	Experiment					Simulation				
	δ/°	a (Å)	b (Å)	γ (°)	A (Å^2)	δ_{sim} (°)	a_{sim} (Å)	b_{sim} (Å)	γ_{sim} (°)	C_{sim}
H1-1	22.0 ± 0.6	**12.3 ± 0.2**	**19.6 ± 0.3**	**89.7 ± 0.7**	**241 ± 7**	22.6	12.3	19.6	90.0	$\begin{pmatrix} 0.562 & 4 \\ -8.079 & 5 \end{pmatrix}$
H1-2	38.0 ± 0.6					40.2	12.3	19.7	90.0	$\begin{pmatrix} -1 & 4.760 \\ -8 & 2.965 \end{pmatrix}$
H1-3	82.0 ± 0.6					81.1	12.2	19.6	90.0	$\begin{pmatrix} -4 & 4.759 \\ -5 & -2.740 \end{pmatrix}$
H2-1	7.1 ± 0.6	**12.6 ± 0.2**	**18.9 ± 0.3**	**89.9 ± 0.5**	**238 ± 7**	8.0	12.6	19.1	90.0	$\begin{pmatrix} 5 & 3.135 \\ -1 & 6.481 \end{pmatrix}$[a]
H2-2	52.9 ± 0.6					53.0	12.5	18.9	90.0	$\begin{pmatrix} 3 & 5.104 \\ -6 & 1.170 \end{pmatrix}$[a]
H2-3	67.1 ± 0.6					66.7	12.6	19.0	90.0	$\begin{pmatrix} 2 & 5.213 \\ -7 & -0.841 \end{pmatrix}$[a]
S-1	34 ± 2	**16.1 ± 0.8**	**16.5 ± 0.8**	**91 ± 2**	**266 ± 26**	33.9	16.2	16.4	91.0	$\begin{pmatrix} -0.586 & 6 \\ -6.758 & 3 \end{pmatrix}$
S-2	56 ± 2					55.8	16.0	16.4	91.0	$\begin{pmatrix} -3 & 6.597 \\ -6 & 0.508 \end{pmatrix}$

Boldly printed data represent lattice constants that are valid for all orientations of the respective phase. Within experimental errors, all relations can be classified as point-on-line coincident with the modeled surface reconstruction lattice.

[a] Matrices, transformed to an appropriate substrate lattice base ($\vec{s}_1$, $\vec{s}_3 = \vec{s}_1 \pm \vec{s}_2$) in which they reflect the point-on-line coincidence by a column of integers.

such single domains are (more or less) point-on-line coincident in all three parts of the alternating surface reconstruction domain sequences, i.e., energetically preferred, while the creation of domain walls as a reaction to the different reconstructed lattice domains underneath would consume energy. It is important to point out that the observed growth cannot be caused by a lattice match with the unreconstructed Au(1 1 1) lattice because calculations in which we used the unreconstructed Au(1 1 1) lattice as substrate lattice did not yield any epitaxial relations which would correspond to the three observed orientations of Phase H1. We, therefore, think that the lattice of the Au(1 1 1) surface reconstruction is the key factor for the observed orientations of the adsorbate layer. This contrasts with the interpretation by Chizov et al. [10] who also observed homogeneously grown PTCDA domains on top of the reconstructed Au(1 1 1) lattice but assume that the surface reconstruction plays no significant role for the orientation of the adsorbate layer.

3.2. PTCDA on reconstructed Au(1 0 0)

LEED images of PTCDA on the reconstructed Au(1 0 0) single crystal show a large number of different orientations of a herringbone phase. Unlike for PTCDA on Au(1 1 1), we find no dependence of the observed orientations on the deposition rate used upon sample preparation, nor do we observe significant changes for different PTCDA layer thicknesses (tested for 0.5–5 ML). A LEED image of a sample with ~5 ML PTCDA prepared using the higher deposition rate of 2.5 ML/min is presented in Fig. 7.

The spots in this image can be explained by four symmetry equivalent domains of five orientations of a herringbone phase, denoted as H-1–H-5. There are four symmetry equivalent domains because each of the two possible domains of the twofold (5×27) surface reconstruction [29] provides a mirror plane which doubles the number of domains of a general epilayer orientation. However, some of the symmetry equivalent domains of

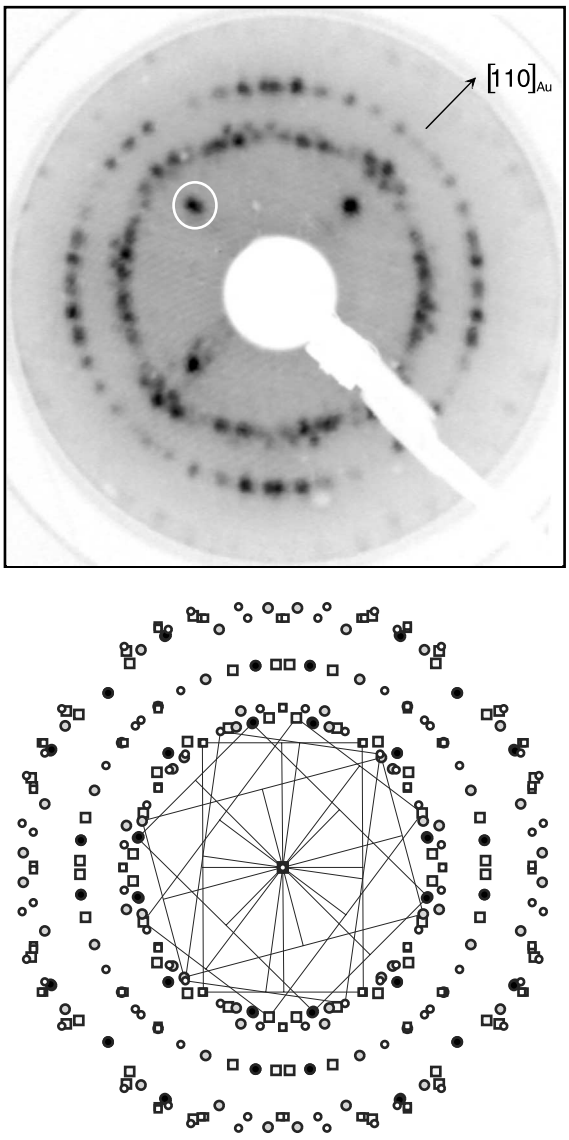

Fig. 7. LEED image obtained at an energy of $E_0 = 9.6$ eV from a 5 ML PTCDA on Au(1 0 0) sample prepared with a deposition rate of 2.5 ML/min. The bright inner spots (one is marked with a white circle) are multiple scattering diffraction features of the Au(1 0 0) surface reconstruction. The adsorbate diffraction spots can be explained by four symmetrically equivalent domains of five herringbone phase orientations H-1(●), H-2(□), H-3(○), H-4(□), and H-5(◎).

the PTCDA herringbone phase are occasionally missing in LEED images (Fig. 7). The reason for the diminishing spot intensity of these domains is the fact that after crystal preparation, the two reconstruction domains sometimes cover uneven surface fractions.

The diffraction patterns show the extinction of $(h\,0)$, $(0\,k)$ diffraction spots for odd values of h and k, characteristic for the p2gg symmetry of the herringbone arrangement. With the angle $\delta = \angle(\vec{a}, \langle 1\,1\,0\rangle_{\mathrm{Au}})$ being used to describe the azimuthal orientation of the adsorbate lattices with respect to the reconstruction lattice, the following angles were obtained from LEED measurements for the orientations H-1–H-5: $\delta_1 = 0.1° \pm 0.7°$, $\delta_2 = 8.0° \pm 0.5°$, $\delta_3 = 36.8° \pm 0.8°$, $\delta_4 = 45.0° \pm 0.8°$, $\delta_5 = 59.3° \pm 0.6°$. Occasionally we find a sixth orientation H-6 with $\delta_6 = 67.5° \pm 0.7°$. Since the corresponding lattice parameters obtained from LEED have overlapping error intervals, H-1–H-6 are assumed to be different orientations of the same phase. The average lattice constants of this phase are: $a = 12.4$ Å, $b = 19.4$ Å, $\Gamma = 90°$; the lattice constants as measured are listed in Table 2 for all orientations. Like it was on Au(1 1 1) we find that the strain values for the herringbone phases on Au(1 0 0) are below 3%. The angle $\delta = \angle(\vec{a}, \langle 1\,1\,0\rangle_{\mathrm{Au}})$ of the listed orientations can, due to the substrate symmetry, only be ambiguously determined as either δ or $|90° - \delta|$. Again, this circumstance requires STM investigations to allow us to decide which of these possible orientations actually occur on the sample. The herringbone phase was successfully identified in STM images like that shown in Fig. 8 and we could verify the angle δ for all orientations, except that for orientation H-3 which we did not find during our STM investigations yet.

Additionally, we again find a square phase with two perpendicularly arranged molecules in the unit cell. A domain of this phase can be seen in Fig. 8. Like it was the case on Au(1 1 1), this phase seems to cover much less surface than the herringbone domains which might explain why we could not identify this phase in LEED images of the investigated samples. The domains of this phase typically have a diameter of about 30 nm, whereas the herringbone phase occurs in large and smooth domains with domain sizes of well over 100 nm. Even at a nominal coverage of PTCDA below 0.5 ML, we do not observe isolated islands of the

Table 2
Lattice parameters of the PTCDA phases found on reconstructed Au(1 0 0), compared to the respective results obtained from the simulation

Phase	Experiment					Simulation				
	$\delta/°$	a (Å)	b (Å)	γ (°)	A (Å^2)	δ_{sim} (°)	a_{sim} (Å)	b_{sim} (Å)	γ_{sim} (°)	C_{sim}
H-1	0.1 ± 0.6	12.6 ± 0.3	19.2 ± 0.4	90.4 ± 0.5	242 ± 11	0.0	12.4	19.1	90.0	$\begin{pmatrix} 4.481 & 0 \\ 4 & 8 \end{pmatrix}$
H-2	8.0 ± 0.5	12.2 ± 0.2	19.7 ± 0.4	90.1 ± 0.5	240 ± 9	7.8	12.1	19.5	90.0	$\begin{pmatrix} 4 & 0.693 \\ -5 & -8.075 \end{pmatrix}$ [a]
H-3	37.0 ± 0.7	12.3 ± 0.3	19.4 ± 0.3	89.6 ± 0.6	239 ± 9	37.3	12.1	19.4	89.8	$\begin{pmatrix} 5 & 3.061 \\ -1 & 6.475 \end{pmatrix}$
H-4	45.0 ± 0.8	12.5 ± 0.3	19.4 ± 0.3	90.4 ± 0.9	242 ± 9	44.3	12.4	19.4	90.0	$\begin{pmatrix} 5 & 3.609 \\ -2 & 5.807 \end{pmatrix}$
H-5	59.3 ± 0.6	12.5 ± 0.2	19.3 ± 0.3	90.2 ± 1	241 ± 8	59.9	12.5	19.2	90.0	$\begin{pmatrix} 0 & 4.538 \\ -8 & -4.011 \end{pmatrix}$ [a]
H-6	67.5 ± 0.7	12.4 ± 0.2	19.4 ± 0.3	89.5 ± 0.8	241 ± 8	68.3	12.2	19.3	90.0	$\begin{pmatrix} 4 & 4.739 \\ -5 & 3.088 \end{pmatrix}$
S-1	4 ± 2	$\mathbf{16.2 \pm 0.8}$	$\mathbf{16.5 \pm 0.8}$	$\mathbf{90 \pm 2}$	$\mathbf{267 \pm 26}$	3.8	16.0	16.5	90.5	$\begin{pmatrix} 6 & 0.443 \\ 3 & 6.879 \end{pmatrix}$
S-2	34 ± 2					33.5	16.1	16.2	89.0	$\begin{pmatrix} 3 & 3.702 \\ -6 & 5.709 \end{pmatrix}$ [a]
S-3	47 ± 2					46.0	16.6	16.8	89.5	$\begin{pmatrix} 6.688 & 5 \\ -1.754 & 5 \end{pmatrix}$
S-4	56 ± 2					56.8	16.1	16.5	89.0	$\begin{pmatrix} 6 & 5.619 \\ -3 & 3.873 \end{pmatrix}$
S-5	74 ± 2					74.0	16.6	16.8	91.5	$\begin{pmatrix} 5 & 6.671 \\ -5 & 1.754 \end{pmatrix}$

Boldly printed data represent lattice constants valid for all orientations of the respective phase. Within experimental errors, all can be classified as point-on-line coincident with the modeled reconstruction lattice.

[a] Matrices, transformed to an appropriate substrate lattice base ($\vec{s}_1$, $\vec{s}_3 = \vec{s}_1 \pm \vec{s}_2$) in which they reflect the point-on-line coincidence by a column of integers.

square phase. Instead, this phase only seems to coexist with the herringbone phase, in a way that it grows in small domains at the domain boundaries of herringbone phase domains.

Boundaries separating the two different motifs usually form a perfect straight line along the {1 1} azimuths of both phases (Fig. 9). These {1 1} azimuths (the diagonals) of the square phase and the herringbone phase are not only parallel to each other, but the lengths of the respective {1 1} vectors (23 Å) are also equal within the experimental error. In Fig. 9 two different orientations of the square phase can be seen, each of them sharing one of the two possible {1 1} azimuths of the herringbone phase. So far we found square phase domains sharing their {1 1} azimuth with one {1 1} azimuth of the H-2 herringbone phase orientation and with both {1 1} azimuths of the orientations H-4 and H-5, i.e., we observed five different orientations of the square phase with respect to the Au(1 0 0) substrate. Several times we found lines of defects within the herringbone phase domains (white lines in Fig. 8) which exhibit a molecular arrangement similar to that of the square phase. In Fig. 8 this can be seen for the herringbone phase orientation H-5. Although the common lattice spacing in conjunction with the characteristic phase boundaries could suggest a possibility to transform the two phases into each other, we did not observe any tip-induced changes, even after scanning several times at the same sample location.

The square phase was measured in scaled STM images exclusively, yielding the following lattice parameters: $a = 16.2 \pm 0.8$ Å, $b = 16.5 \pm 0.8$ Å,

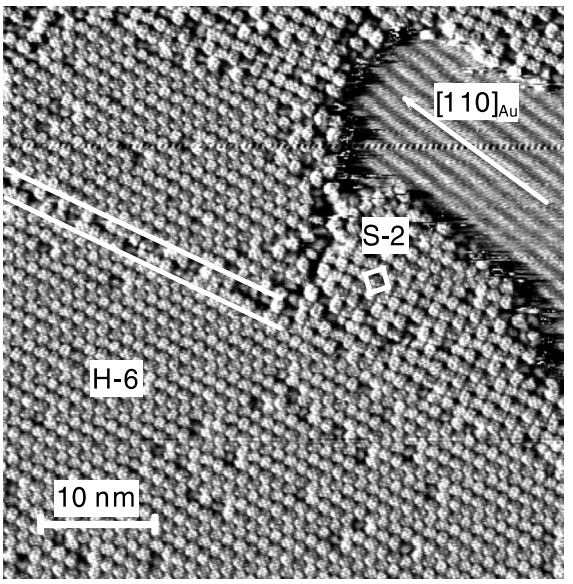

Fig. 8. STM image of a 1–2 ML sample of PTCDA on reconstructed Au(1 0 0) prepared with a deposition rate of 2.5 ML/min. The trenches in the reconstructed gold layer running along the [1 1 0] direction can be seen as a pattern of dark stripes in the upper right corner. Besides the herringbone Phase H-6, a domain adopting the square arrangement of PTCDA molecules can be seen in the upper part. Occasionally we found defect lines (marked by white lines in the left part of the image) which extend into the herringbone domains and show a arrangement of molecules similar to that of the square phase [$U = 0.9$ V, $I = 0.13$ nA].

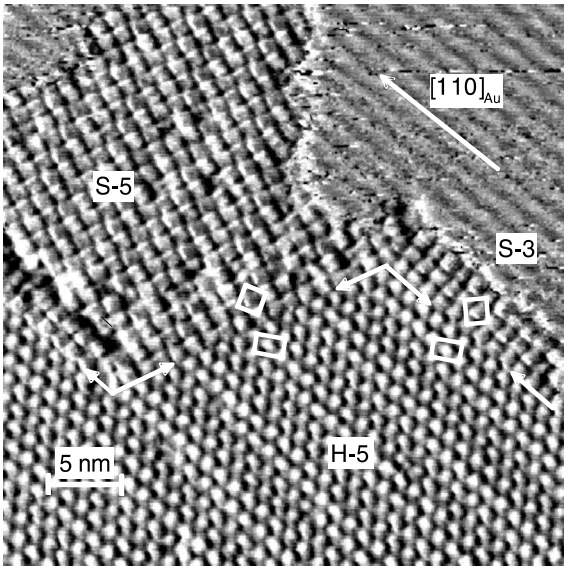

Fig. 9. STM image of a nominal coverage of 1 ML PTCDA on reconstructed Au(1 0 0), prepared with a deposition rate of 0.5 ML/min. The pattern of dark stripes in the upper right corner correspond to the trenches in the reconstructed gold layer running along the [1 1 0] direction. There are two orientations of the square phase growing in small domains adjacently to the herringbone phase H-5. The white rectangles symbolise the respective unit cells of the square phase and the herringbone phase. The straight and sharp domain boundaries separating the square phase domains from the herringbone phase domains are always parallel to one diagonal ({1 1} azimuth) of both phases. In the STM image these domain boundaries are indicated by white arrows [$U = 0.75$ V, $I = 0.05$ nA].

$\Gamma = 90° \pm 2°$. Although the error of measurements in scaled STM images is estimated to be significantly larger compared to that of LEED measurements, these lattice parameters are believed to be rather precise because sterical modeling just allows to place two flat lying molecules perpendicularly (respective molecule axes are perpendicular) in this unit cell, provided that the van-der-Waals radii do not significantly overlap.

Now we will discuss the observed orientations and the azimuthal relation of the adsorbate lattices with the reconstructed lattice to decide whether there is a similar kind of determination of the adsorbate layer orientation by the substrate lattice, as found for PTCDA on Au(1 1 1). The Au(1 0 0) surface reconstruction can be modeled as a slightly distorted hexagonal lattice $\mathrm{Au}(1\,0\,0)_{\mathrm{hex}}$. Very accurate X-ray scattering studies [30] revealed that the small scale structure of the reconstruction can be described with the following unit cell parameters: $|\vec{s}_1| = 2.763 \pm 0.002$ Å, $|\vec{s}_2| = 2.766 \pm 0.002$ Å and $\angle(\vec{s}_1, \vec{s}_2) = 120.03° \pm 0.1°$, with $\vec{s}_1$ being aligned with the long axis of the actual (5×27) unit cell. This $(\vec{s}_1, \vec{s}_2)$ lattice was used to describe the reconstruction lattice in our calculations, carried out analogously to those for PTCDA on Au(1 1 1).

Like there, we find no commensurism or point-on-point coincidence of the hypothetical adsorbate lattice with the modeled lattice of the surface reconstruction within the scanned lattice parameter range, but obtain point-on-line epitaxial relations for all orientations of the herringbone phase and the square phase, which are consistent with the measured angles and lattice parameters (Fig. 10).

Calculations for which we used the unreconstructed Au(1 0 0) lattice instead of the $Au(1\,0\,0)_{hex}$ lattice do not yield any epitaxial relation which would be compatible with the observed herringbone phase orientations. This fact suggests that again the surface reconstruction of Au(1 0 0) is determinant for the observed domain orientations in the PTCDA layer. The values in Table 2 were again selected from the simulation results according to their correspondence with the experimentally obtained lattice parameters.

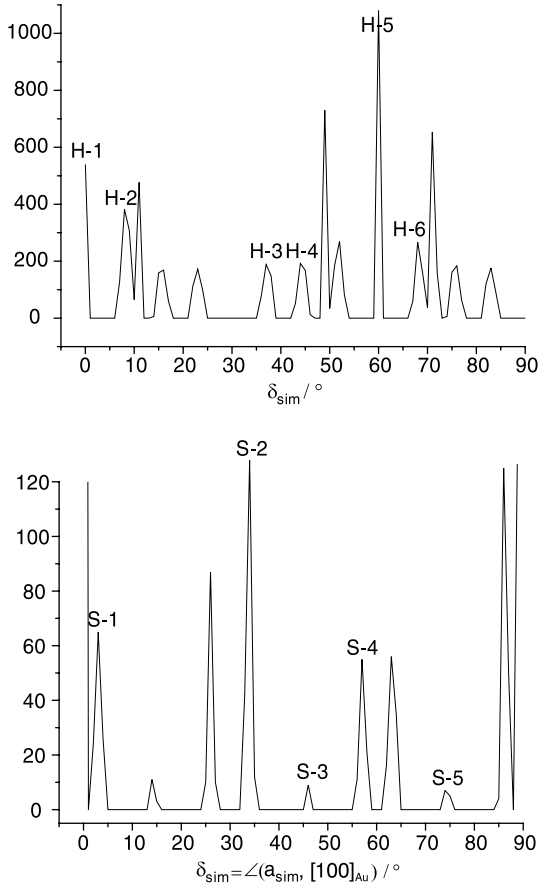

Fig. 10. Histogram showing the point-on-line coincident solutions found for the herringbone phase (upper chart) and the square phase (lower chart) of PTCDA on reconstructed Au(1 0 0). The scanned adsorbate lattice parameter range for the herringbone phases was: $a_{sim} = 12.0$–12.6 Å, $b_{sim} = 19.0$–19.8 Å, $\Gamma_{sim} = 89.0$–$91.0°$. In case of the square phase, the lattice constants were varied between: $a_{sim} = 16.0$–16.8 Å, $b_{sim} = 16.0$–16.8 Å, $\Gamma_{sim} = 88.5$–$91.5°$. The peaks are labeled according to the respective phase and the index of the angle δ.

4. Summary

The growth of PTCDA on Au(1 1 1) and Au(1 0 0) single crystals was investigated by LEED and STM in UHV. For PTCDA on Au(1 1 1), LEED investigation reveals the growth of two herringbone phases which are found to adsorb in single domains homogeneously on top of the 120° alternating domain sequences of the Au(1 1 1) surface reconstruction. One of them is observed in samples prepared with higher molecular flux only. This homogeneous adsorption on top of multiple reconstruction domains requires the azimuthal relation with respect to the substrate lattice to be described by three angles for each of the two phases. All of the resulting six orientations are point-on-line coincident with the lattice of the reconstructed Au(1 1 1) surface, hence energetically favorable. This explains the growth in large domains despite the fact that there are multiple reconstruction domains underneath. In addition, two orientations of a square phase, which grow in small islands on single reconstruction domains, are found to be point-on-line coincident as well.

The LEED images of PTCDA on reconstructed Au(1 0 0) reveal six orientations of a herringbone phase which is also observed in STM images. A square phase with two different orientations is exclusively found in STM images, but not in LEED images due to the small surface fraction covered by this structure. Similar to the structures found on Au(1 1 1), the epitaxial relations of all observed orientations on Au(1 0 0), including those of the square phase, can be classified as point-on-line coincident.

The herringbone phase of PTCDA has been reported to grow on Au(1 0 0) previously, but STM investigations revealed the growth of completely different orientations on unreconstructed islands of the gold surface [7]. We have shown that the growth of this phase seems to be related to the underlying surface reconstruction as well. The square phase of PTCDA which was not reported for Au(1 0 0) yet, was found to coexist with the

herringbone phase as kind of herringbone "surface" reconstruction; it could also be classified as point-on-line coincident with the reconstructed surface lattice. The rod-like structure of PTCDA, formed by upright standing PTCDA molecules [7], could not be observed on the Au(1 0 0) single crystal.

The consideration of the reconstructed surface lattice turned out to be crucial for an explanation of the growth of PTCDA on Au(1 1 1) and Au(1 0 0) single crystals within the limits of geometrical lattice match. Our simulation results support the interpretation that the total interfacial energy of the PTCDA layer on gold single crystalline substrates is generally minimized by point-on-line coincident adsorption.

References

[1] M.A. Herman, H. Sitter, Molecular Beam Epitaxy, Springer, Berlin, 1989.
[2] A. Hoshino, S. Isoda, H. Kurata, T. Kobayashi, J. Appl. Phys. 76 (7) (1994) 4113.
[3] A. Hoshino, S. Isoda, H. Kurata, T. Kobayashi, Y. Yamashita, Jpn. J. Appl. Phys. 34 (1995) 3858.
[4] C. Ludwig, B. Gompf, W. Glatz, J. Petersen, W. Eisenmenger, M. Möbus, U. Zimmermann, N. Karl, Zor. Phys. B.-Condens. Matter 86 (1992) 397.
[5] S.R. Forrest, P.E. Burrows, E.I. Haskal, F.F. So, Phys. Rev. B 49 (16) (1994) 11309.
[6] C. Kendrick, A. Kahn, S.R. Forrest, Appl. Surf. Sci. 104/105 (1996) 586.
[7] T. Schmitz-Hübsch, T. Fritz, R. Staub, A. Back, N.R. Armstrong, K. Leo, Surf. Sci. 437 (1999) 166.
[8] T. Schmitz-Hübsch, T. Fritz, F. Sellam, R. Staub, K. Leo, Phys. Rev. B 55 (1997) 7972.
[9] P. Fenter, F. Schreiber, L. Zhou, P. Eisenberger, S.R. Forrest, Phys. Rev. B 56 (1997) 3046.
[10] I. Chizov, A. Kahn, G. Scoles, J. Cryst. Growth 208 (2000) 449.
[11] C. Seidel, J. Poppensieker, H. Fuchs, Surf. Sci. 408 (1998) 223.
[12] T.J. Schuerlein, A. Schmidt, P.A. Lee, K.W. Nebesny, N.R. Armstrong, Jpn. J. Appl. Phys. 34 (7B) (1995) 3837.
[13] U. Zimmermann, N. Karl, Surf. Sci. 268 (1992) 296.
[14] M. Möbus, N. Karl, Thin Solid Films 215 (1992) 213.
[15] M. Möbus, M. Schreck, N. Karl, Thin Solid Films 175 (1989) 89.
[16] F. Sellam, T. Schmitz-Hübsch, M. Toerker, S. Mannsfeld, H. Proehl, T. Fritz, K. Leo, Surf. Sci. 478 (2001) 113.
[17] C. Seidel, Charakterisierung organischer Adsorbate auf Silbereinkristallen mit den Meßmethoden LEED und STM, Ph.D. Thesis, University of Stuttgart, 1993.
[18] C. Seidel, C. Awater, X. Liu, R. Ellerbrake, H. Fuchs, Surf. Sci. 371 (1997) 123.
[19] K. Glöckler, C. Seidel, A. Soukopp, M. Sokolowski, E. Umbach, M. Böhringer, R. Berndt, W. Schneider, Surf. Sci. 405 (1998) 1.
[20] R. Staub, M. Toerker, T. Fritz, T. Schmitz-Hübsch, F. Sellam, K. Leo, Surf. Sci. 445 (2000) 368.
[21] D.E. Hooks, T. Fritz, M.D. Ward, Adv. Mater. 13 (2001) 227.
[22] C. Günther, Organische Molekularstrahlepitaxie: Ordnungsprinzipien großer Aromaten auf Schichthalbleitern, LOGOS Verlag, Berlin, 1998.
[23] T. Ogawa, K. Kuwamoto, S. Isoda, T. Kobayashi, N. Karl, Acta. Cryst. Sect. B 55 (1999) 123.
[24] T. Fritz, Molecular Architecture in Heteroepitaxially Grown Organic Thin Films, s.f.p.s. Wissenschaftlicher Fachverlag, Dresden, 1999.
[25] A.C. Hillier, M.D. Ward, Phys. Rev. B 54 (1996) 14037.
[26] T. Fritz, in preparation.
[27] R.J. Needs, M. Mansfield, J. Phys.: Condens. Matter 1 (1989) 7555.
[28] J.V. Barth, H. Brune, G. Ertl, R.J. Behm, Phys. Rev. B 42 (1990) 9307.
[29] X. Gao, A. Hamelin, M.J. Weaver, Phys. Rev. B 46 (1992) 7096.
[30] D. Gibbs, B.M. Ocko, D.M. Zehner, S.G.J. Mochrie, Phys. Rev. B 42 (12) (1990) 7330.